Catalysis Science & Technology

Reductive CO_2 Fixation by *N*-Formylation Reaction over Supported Pt Nanoparticle Catalyst Modified with Basic Polyoxometalates

Journal:	*Catalysis Science & Technology*
Manuscript ID	CY-ART-12-2024-001513.R1
Article Type:	Paper
Date Submitted by the Author:	22-Feb-2025
Complete List of Authors:	Kikkawa, Soichi; Tokyo Metropolitan University Matsunaga, Yutaro; Tokyo Metropolitan University Fukuda, Shoji; Tokyo Metropolitan University - Minamiosawa Campus, Department of Chemistry, Graduate School of Science Yamazoe, Seiji; Tokyo Metropolitan University, Department of Chemistry

ARTICLE

Reductive CO_2 Fixation by *N*-Formylation Reaction over Supported Pt Nanoparticle Catalyst Modified with Basic Polyoxometalates

Received 00th January 20xx,
Accepted 00th January 20xx

DOI: 10.1039/x0xx00000x

Soichi Kikkawa,*[a] Yutaro Matsunaga,[a] Shoji Fukuda,[a] and Seiji Yamazoe*[a]

N-formylation reaction of amines using CO_2 as a carbon source is a promising way to utilize CO_2 to produce value-added chemicals. We herein developed supported Pt nanoparticle (NP) catalysts with a surface modified with a basic polyoxometalate, $[Nb_6O_{19}]^{8-}$, by a simple adsorption method. The designed surface efficiently promoted the reductive CO_2 fixation by *N*-formylation reaction of secondary amines under CO_2 and H_2 conditions. The interface between the modified basic $[Nb_6O_{19}]^{8-}$ and Pt NP surface facilitated the hydrogenation of carbamate intermediates by the bifunctionality of H_2 activation and basicity. This work demonstrated that Pt NP surface design by a bottom-up modification with basic polyoxometalates facilitated *N*-formylation reaction using CO_2 as a carbon source without the addition of any external base.

Introduction

The concentration of atmospheric carbon dioxide (CO_2) is increasing year by year and the climate is deteriorating, although the relationship between CO_2 concentration and climate is still under debate. Against this background, it is increasingly important to reduce the atmospheric CO_2 concentration by developing technology to capture and use CO_2 as a C1 building block.[1] Among such technologies, much attention has focused on CO_2 fixation into chemicals to produce value-added chemicals such as carbonates, formamides, carboxylic acids, ureas, and methylated products from the abundant and cheap CO_2.[2-8] In particular, formamides are widely applied in industry as raw materials. *N*-Formylation of amines to produce formamides is facilitated by reducing and carbonylation agents; however, toxic CO and phosgene have been employed as carbon sources. In recent years, the reductive *N*-formylation reaction has thus attracted attention to use CO_2 as a carbon source instead of the direct insertion of CO.[9-15] This reaction is facilitated by H_2 as a reducing agent, which is atomic-economically more favored than organic silicones and only produces H_2O as a by-product.

The *N*-formylation reaction utilizing CO_2 as a carbon source requires the activation of H_2 and the hydrogenation of carbamate intermediates, which are easily formed from amine with CO_2 under a high CO_2 pressure.[10, 11, 13, 15] Actually, the catalysts reported in homogeneous systems are equipped with two kinds of active sites for interaction with carbamate intermediates and for the activation of H_2.[10] Because of easy collection and regeneration for practical use, heterogeneous catalysts have been developed, of which active metal nanoparticles (NPs) such as Co,[9] Cu,[16] Pd,[17] Pt,[7] Au,[18, 19] and Ir[13, 15] were dispersed on support materials. Bimetallic alloy NPs were reported to afford the bifunctional role of hydrogenation and interaction with the intermediates.[17] Interfacial sites between metal NPs and the oxide support are also active for the efficient *N*-formylation reaction.[16] For some systems, it was reported that the addition of a base is effective to promote the *N*-formylation reaction.[10, 11] As mentioned above, the design of active sites of supported metal NP catalyst is essential to efficiently facilitate reductive CO_2 fixation by the *N*-formylation reaction.

Composite materials of metal NPs with polyoxometalates (POMs) as protecting ligands have attracted attention because of their unique functionalities.[20-26] POMs that consist of dozens of metal-oxo units coordinated to the surface of metal NPs due to the electronegativity of surface oxygen atoms and electronically interacted with the surface of metal NPs. POM–metal NP composites have been widely applied, such as $[SiW_{11}O_{39}]^{8-}$,[20, 21] $[P_2W_{18}O_{62}]^{7-}$,[26] $[AlW_{11}O_{39}]^{9-}$,[22] $[P_2W_{18}O_{62}]^{6-}$,[20, 26] and $[Nb_6O_{19}]^{8-}$.[21] We found that V-group POMs such as $[Nb_6O_{19}]^{8-}$,[27, 28] $[Ta_6O_{19}]^{8-}$,[27] and $[Nb_{10}O_{28}]^{6-}$ [29, 30] showed base catalytic activity for Knoevenagel condensation and CO_2 fixation reactions. In particular, $[Nb_6O_{19}]^{8-}$ showed strong superbase catalysis for proton abstraction from C–H having pK_a above 26.[28] Recently, we applied these basic POMs to modify the Al_2O_3-supported Au NP catalyst and found that the design of a high-density POM–metal NP interface afforded highly efficient hydrogenation of aromatic nitro compounds.[23] Basic active sites of POMs stabilized the nitrophenolate intermediates, and the electronegative Au NP surface and the interfacial sites of the POM–metal NP surface facilitated H_2 activation, leading to highly efficient hydrogenation of nitrophenolate intermediates. POMs were highly selectively modified on the surface of Au NPs by a simple adsorption method and the size distribution of Au NPs was maintained even after the modification. Such a

[a] *Department of Chemistry, Graduate School of Science, Tokyo Metropolitan University, 1-1 Minami-Osawa, Hachioji, Tokyo 192-0397, Japan*

† Footnotes relating to the title and/or authors should appear here.
Supplementary Information available: [details of any supplementary information available should be included here]. See DOI: 10.1039/x0xx00000x

bottom-up modification enables us to design the surface of supported metal NP catalysts while maintaining the nature of the NPs, such as their size and shape.

In this study, the surface of supported Pt NPs loaded on an Al_2O_3 support was decorated with basic POMs by an adsorption method, which were applied to the reductive *N*-formylation reaction of piperidine using CO_2 as a carbon source. Our group has reported that *N*-formylation of various amines including piperidine proceeds under a CO_2 and H_2 atmosphere by using a Pt-containing Nb-based POM, $[Pt(Nb_6O_{19})_2]^{12-}$, as a catalyst.[7] Pt NPs modified with POMs were formed during the reaction; it was thus considered that the bifunctional catalysis of the basicity of POMs and the H_2-activation property of Pt NPs promoted the *N*-formylation reaction. In this study, supported Pt NP catalysts modified with basic POMs ($[M_6O_{19}]^{8-}$, M = Nb, Ta) were designed by controlling the concentration of $K_8M_6O_{19}$ aq. for the adsorption method. The Pt NP surface designed by a bottom-up modification with basic POMs facilitated the *N*-formylation reaction using CO_2 as a carbon source without the addition of any external base.

Results and Discussion

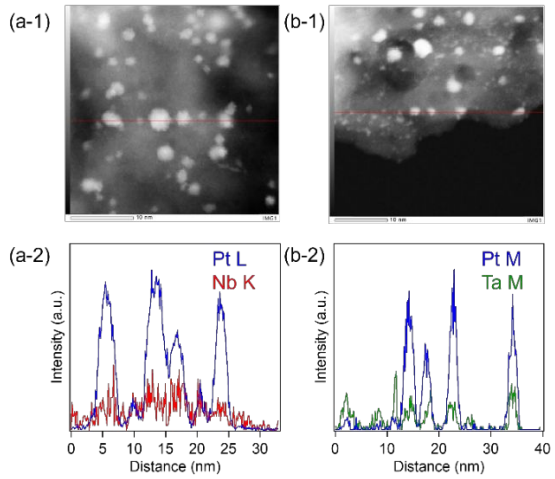

Figure 1. HAADF-STEM images of (a-1) **4.0Nb6-Pt/Al_2O_3** and (b-1) **4.0Ta6-Pt/Al_2O_3**. (a-2) EDX analysis of **4.0Nb6-Pt/Al_2O_3** from Nb K-edge (red) and Pt L-edge (blue). (b-2) EDX analysis of **4.0Ta6-Pt/Al_2O_3** from Ta M-edge (green) and Pt M-edge (blue).

Supported Pt NPs loaded on Al_2O_3 support (**Pt/Al_2O_3**) were prepared by an impregnation method, followed by calcination and H_2 reduction. **Pt/Al_2O_3** was dispersed in an aqueous solution of basic $K_8M_6O_{19}$ (M = Nb and Ta) and then dried in a vacuum. STEM images of **Pt/Al_2O_3** showed that Pt NPs were highly dispersed on Al_2O_3 support and the mean particle size was 1.5 nm (**Figure S1a**). CO pulse titration also showed a similar particle size with 58% dispersion. After modification with $[Nb_6O_{19}]^{8-}$ (**4.0Nb6-Pt/Al_2O_3**) and $[Ta_6O_{19}]^{8-}$ (**4.0Ta6-Pt/Al_2O_3**) in excess $K_8M_6O_{19}$ aq., the average particle sizes hardly changed (**Figure S1b** and **Figure S1c**). EDX line analysis of **4.0Nb6-Pt/Al_2O_3** showed that Pt L- and Nb K-edge fluorescent X-rays were detected at similar locations, indicating that $[Nb_6O_{19}]^{8-}$ clusters were highly selectively deposited on the Pt NP surface (**Figure 1a**). **4.0Ta6-Pt/Al_2O_3** also showed similar highly selective adsorption of $[Ta_6O_{19}]^{8-}$ (**Figure 1b**). The amounts of CO adsorbed by pulse titration were decreased by the $[Nb_6O_{19}]^{8-}$ and $[Ta_6O_{19}]^{8-}$ modification over **4.0Nb6-Pt/Al_2O_3** and **4.0Ta6-Pt/Al_2O_3**. Thus, part of the Pt NP surface was covered by POMs (**Table 1**).

Table 1. Loadings of POMs and CO adsorbed on Pt surface determined by ICP analysis and CO pulse titration, respectively.

Sample	$K_8M_6O_{19}$/Pt	Pt (wt%)	POM (wt_M%)	$[M_6O_{19}]^{8-}$ ($\mu mol/g_{cat}$)	Exposed Pt ($\mu mol/g_{cat}$)
4.0Nb6-Pt/Al_2O_3	4.0	4.6	0.89	14	135
1.0Nb6-Pt/Al_2O_3	1.0	4.6	0.97	22	128
0.5Nb6-Pt/Al_2O_3	0.5	4.7	1.38	23	133
0.1Nb6-Pt/Al_2O_3	0.1	4.7	0.60	12	138
0.06Nb6-Pt/Al_2O_3	0.06	4.7	0.47	8.5	142
0.03Nb6-Pt/Al_2O_3	0.03	4.7	0.22	3.9	145
0.006Nb6-Pt/Al_2O_3	0.006	4.7	0.036	0.6	147
4.0Ta6-Pt/Al_2O_3	4.0	4.4	3.6	31	25
Pt/Al_2O_3	-	4.7	-	-	145

Pt L_3-edge X-ray absorption fine structure (XAFS) spectra revealed that the interaction between Pt NP surface and modified $[Nb_6O_{19}]^{8-}$ (**Figure S2**). X-ray absorption near edge structure (XANES) showed an increase in white line peak intensity by modification of $[Nb_6O_{19}]^{8-}$, where the intensity was influenced by the modified amount of $[Nb_6O_{19}]^{8-}$, indicating the electronic modulation of Pt by $[Nb_6O_{19}]^{8-}$. Fourier transform (FT) of extended X-ray absorption fine structure (EXAFS) spectra showed the presence of the scattering peak of Pt–O in **4.0Nb6-Pt/Al_2O_3** other than that of Pt–Pt, while **Pt/Al_2O_3** mainly showed the peak of Pt–Pt. Since the STEM images suggested that the particle size of Pt NPs maintained through the $[Nb_6O_{19}]^{8-}$ modification, the white line peak increase in XANES spectra and Pt–O scattering peak in FT of EXAFS spectra were owing to the addiction oxygen atom on Pt NP surface. Those indicated that the coordination of oxygen atoms of $[Nb_6O_{19}]^{8-}$ on Pt NP surface.

Nb K-edge XAFS revealed the structure of modified $[Nb_6O_{19}]^{8-}$. FT of EXAFS spectra of **4.0Nb6-Pt/Al_2O_3** showed the scattering peaks of Nb–O and Nb–O–Nb, as shown in $K_8Nb_6O_{19}$ aq. precursor (**Figure 2a**). **4.0Ta6-Pt/Al_2O_3** also showed that the Ta–O and Ta–O–Ta scattering peaks were retained in FT of Ta L_3-edge EXAFS spectra (**Figure S3**). These findings indicate that the modified clusters maintained the Lindqvist-type structure. The base property of adsorbed POMs was confirmed by the coloration of *p*-nitrophenol to form phenoxide ion under basic conditions (**Figure 2b**). The suspension of **4.0Nb6-Pt/Al_2O_3** or **4.0Ta6-Pt/Al_2O_3** showed the color change to yellow as observed in the MeOH solution of *p*-nitrophenol with the addition of $K_8Nb_6O_{19}$.

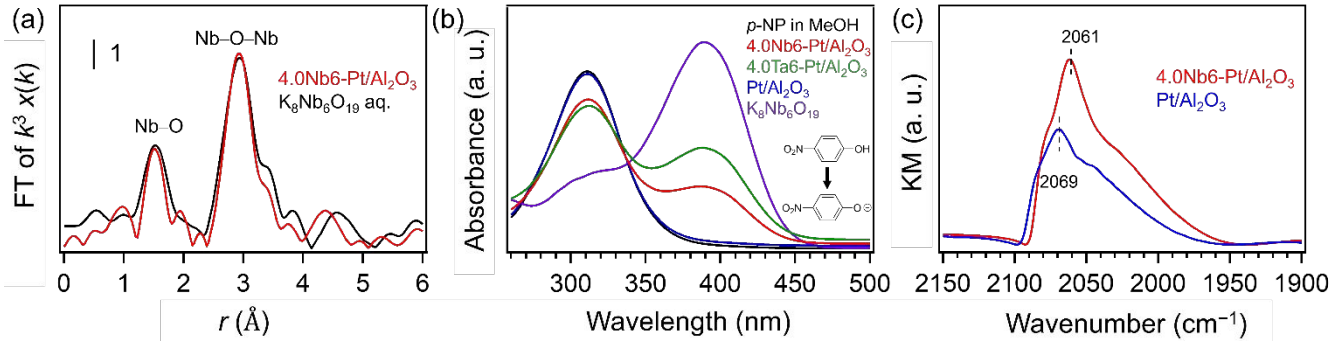

Figure 2. (a) FT of Nb K-edge EXAFS spectra of **4.0Nb6-Pt/Al_2O_3** (red) and $K_8Nb_6O_{19}$ aqueous solution (black). (b) UV-vis spectra of *p*-nitrophenol in MeOH solution (black) and that dispersed with **Pt/Al_2O_3** (blue), **4.0Nb6-Pt/Al_2O_3** (red), **4.0Ta6-Pt/Al_2O_3** (green), and $K_8Nb_6O_{19}$ (purple). (c) IR-DRIFTS spectra of **Pt/Al_2O_3** (blue) and **4.0Nb6-Pt/Al_2O_3** (red) under 5% CO/He. The samples were pretreated under O_2 at 673 K for 15 min and then 5% H_2/He at 673 K for 15 min.

IR-DRIFTS spectra using CO as a probe showed the C–O stretching vibration of on-top adsorbed CO species on the Pt surface. The absorption band of CO species was observed even after modification of $[Nb_6O_{19}]^{8-}$ and shifted from 2069 cm^{-1} to 2061 cm^{-1} (**Figure 2c**). This low-frequency shift of on-top CO species compared to bare Pt NP surface of **Pt/Al_2O_3** indicated the electronic modulation of Pt modified by $[Nb_6O_{19}]^{8-}$.[31, 32] Thus, we consider that the oxygen atoms coordinated to the Pt NP surface, as described in our previous reports on Au NPs modified with $[Nb_6O_{19}]^{8-}$.[23]

As for a series of ***X*Nb6-Pt/Al_2O_3**, the loadings of POMs by ICP analysis and exposed Pt surface by CO pulse titration are summarized in **Table 1**. The loadings of $[Nb_6O_{19}]^{8-}$ increased with increasing concentration of $K_8Nb_6O_{19}$ aq., while the adsorbed CO amount slightly decreased with increasing loadings of $[Nb_6O_{19}]^{8-}$. At $[Nb_6O_{19}]^{8-}$/Pt ratios above 0.5, the loadings of $[Nb_6O_{19}]^{8-}$ reached a plateau. At $[Nb_6O_{19}]^{8-}$/Pt ratios of 4.0, the amount of modified $[Nb_6O_{19}]^{8-}$ decreased, which would be owing to the leaching out of Pt species occurred at highly basic condition. From CO pulse titration, the Pt NPs were highly covered with $[Ta_6O_{19}]^{8-}$ in $K_8Ta_6O_{19}$ aq. We have reported that the surface oxygen atoms of $[Ta_6O_{19}]^{8-}$ possessed higher negative charge than those of $[Nb_6O_{19}]^{8-}$.[27] We consider that this negative charge of surface oxygen atoms of $[Ta_6O_{19}]^{8-}$ leads to a large amount of $[Ta_6O_{19}]^{8-}$ being adsorbed to the Pt NP surface in **4.0Ta6-Pt/Al_2O_3**.

The POM-modified Pt NPs catalysts were applied to *N*-formylation reaction using CO_2 as a carbon source, where basic reagents are required for CO_2 activation (**Scheme 1**). **Figure 3** shows the product yields in the *N*-formylation reaction of piperidine under CO_2 and H_2 atmosphere. The yield of 1-formylpiperidine increased by the modification of **Pt/Al_2O_3** with $[Nb_6O_{19}]^{8-}$ and $[Ta_6O_{19}]^{8-}$, where the product yield over **4.0Nb6-Pt/Al_2O_3** was slightly higher than that over **4.0Ta6-Pt/Al_2O_3**. The addition of Cs_2CO_3 or $K_8Nb_6O_{19}$ aq. as a base to **Pt/Al_2O_3** also increased the activity while acidic Nb_2O_5 and weak base NH_4Cl hardly improved the activity of **Pt/Al_2O_3**. Those suggested that the modified basic POMs played an important role in the reaction. The product yield increased with elongation of the reaction time (**Figure 4b**) and reached to almost the full conversion. Thus, the *N*-formylation reaction of piperidine catalytically proceeded over **4.0Nb6-Pt/Al_2O_3**.

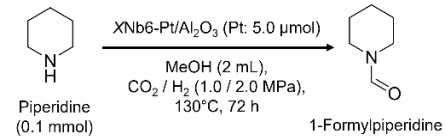

Scheme 1. *N*-Formylation of piperidine using CO_2 as a carbon source.

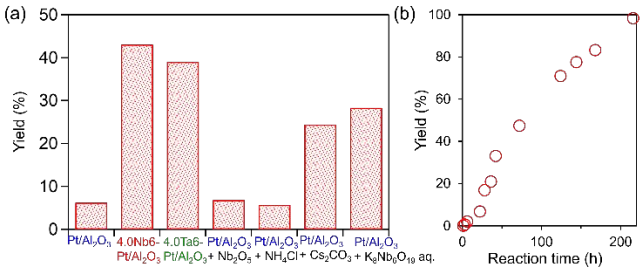

Figure 3. (a) Product yield in *N*-formylation reaction of piperidine using CO_2 with various catalysts. (b) Product yield as a function of reaction time. Reaction conditions: piperidine, 0.1 mmol; methanol, 2 mL; catalyst, 19.5 mg; internal standard, dodecane; CO_2, 1.0 MPa; H_2, 2.0 MPa; reaction temperature, 130°C; reaction time, 72 h.

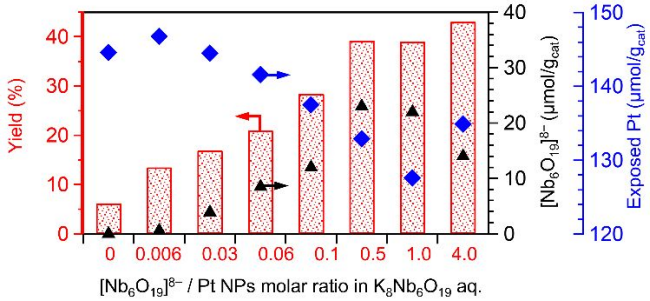

Figure 4. Product yields for *N*-formylation of piperidine over ***X*Nb6-Pt/Al_2O_3** as a function of $[Nb_6O_{19}]^{8-}$ / Pt NPs molar ratio in $K_8Nb_6O_{19}$ aq. Loadings of Nb species revealed by ICP measurements (black right axis) and adsorbed exposed Pt atoms by CO pulse measurements (blue right axis). Reaction conditions: piperidine, 0.1 mmol; methanol, 2 mL; catalyst, 19.5 mg; internal standard, dodecane; CO_2, 1.0 MPa, H_2, 2.0 MPa; reaction temperature, 130°C; reaction time, 72 h.

Next, the effect of surface coverage of Pt NPs by $[Nb_6O_{19}]^{8-}$ on the catalytic activity was investigated. **Figure 4** summarizes the activities for *N*-formylation reaction of piperidine using CO_2 over ***X*Nb6-Pt/Al_2O_3**. **Pt/Al_2O_3** was dispersed in various concentrations of $K_8Nb_6O_{19}$ aq. to modify the Pt NP surface with $[Nb_6O_{19}]^{8-}$. The

yield of 1-formylpiperidine reached twice by the modification of $[Nb_6O_{19}]^{8-}$ to **Pt/Al$_2$O$_3$** in a low concentration of $K_8Nb_6O_{19}$ aq. ($[Nb_6O_{19}]^{8-}$/Pt molar ratio was 0.006, referred as **0.006Nb6-Pt/Al$_2$O$_3$**). The product yield increased with increasing the concentration of $K_8Nb_6O_{19}$ aq., and plateaued at $[Nb_6O_{19}]^{8-}$/Pt molar ratios above 0.5. As previously mentioned, the loadings of $[Nb_6O_{19}]^{8-}$ also increased with increasing the concentration of $K_8Nb_6O_{19}$ aq. The adsorbed CO amount decreased with increasing the loadings of basic $[Nb_6O_{19}]^{8-}$. The exposed Pt surface slightly decreased with increasing $[Nb_6O_{19}]^{8-}$ amount but remained even in **4.0Nb6-Pt/Al$_2$O$_3$**. Those indicated that both of the exposed Pt NPs surface and basic $[Nb_6O_{19}]^{8-}$ on the surface are essential for the reaction. Indeed, **4.0Ta6-Pt/Al$_2$O$_3$** that the Pt NPs surface highly covered with $[Ta_6O_{19}]^{8-}$ afforded not higher activity than **4.0Nb6-Pt/Al$_2$O$_3$**. **Table 1** showed that the Pt NP surface was highly covered in **4.0Ta6-Pt/Al$_2$O$_3$**. Thus, the low activity of **4.0Ta6-Pt/Al$_2$O$_3$** would be owing to insufficiency of the exposed Pt surface. The trends in product yield well matched to the Nb loading amount rather than exposed Pt atoms, this suggested that the interfacial sites between Pt NPs and $[Nb_6O_{19}]^{8-}$ were important to promote the *N*-formylation reaction.

We also investigated the modification of Pt NPs loaded on various support such as ZrO_2, Nb_2O_5, and TiO_2 (**Figure S4**). $[Nb_6O_{19}]^{8-}$ modification improved the activity of supported Pt NPs catalysts for *N*-formylation reaction. Among the tested support metal oxides, Al_2O_3 showed the highest dispersion and would result in highest conversion. The modification of $[Nb_6O_{19}]^{8-}$ is more efficient than simply use of basic support such as ZrO_2. This indicated that the bottom-up modification of $[Nb_6O_{19}]^{8-}$ generally improve the activity of Pt NPs for this reaction.

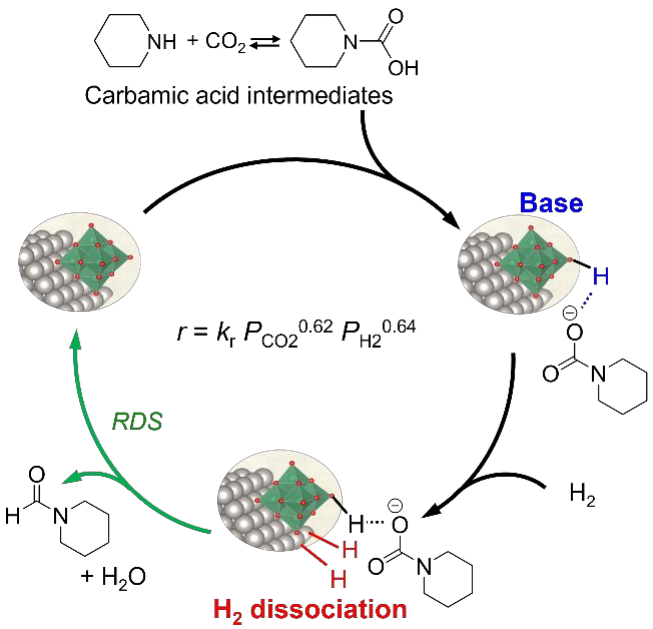

Figure 5. Proposed reaction mechanism of *N*-formylation of piperidine using CO_2 over **Nb6-Pt/Al$_2$O$_3$**.

We have previously reported the mechanism of *N*-formylation reaction using CO_2 over Pt-sandwich-type $[Nb_6O_{19}]^{8-}$ cluster, which formed $[Nb_6O_{19}]^{8-}$-modified Pt NPs on Nb_2O_5 support during reaction.[7] As proposed, piperidine reacted with CO_2 to form carbamic acid during reaction. The carbamic acid interacted with surface oxygen of $[Nb_6O_{19}]^{8-}$, followed by reduction of the C=O bond by Pt NPs at the interface between Pt NPs and $[Nb_6O_{19}]^{8-}$. Other works also reported the mechanism via carbamate intermediates; thus, we consider that the hydrogenation of carbamate intermediates is key step in this reaction.[11, 13, 15] In this study, isotopic experiment using both $^{12}CO_2$ and $^{13}CO_2$ as carbon sources showed the ^{13}C-contained 1-formylpiperidine as a product (**Figure S5**), revealing that CO_2 was utilized as a carbon source. CO was detected in the gas phase analysis when using MeOH as solvent (**Table S2**). The reaction efficiently proceeded when using dimethylamine and toluene as solvents and CO production was suppressed in those cases. Those results indicated that CO was produced as a byproduct and poisoned Pt NP surface during the reaction. Moreover, the reaction order analysis carried out in various CO_2 and H_2 pressures indicated that the reaction rate depended on both for P_{CO2} and P_{H2}, and the reaction orders for P_{CO2} and P_{H2} are 0.62 and 0.64, respectively (**Figure S6**). Based on the above results, the carbamate/carbamic acid were intermediate species. The carbamate intermediates were stabilized at the basic sites of $[Nb_6O_{19}]^{8-}$ on Pt NP surface and then hydrogenated to 1-formylpiperidine, which includes formation of carbamate/carbamic acid, adsorption of carbamate species on the base sites, dissociation of H_2 on Pt NP surface, and hydrogenation of the carbamate intermediates (**Figure 5**). The activity dependence on P_{CO2} and P_{H2} suggested that plausible rate-determining step for this reaction is not supply of CO_2 or H_2, and would be the reduction of carbamate intermediates by dissociated hydrogen on Pt species. We concluded that the interface between Pt NPs and basic $[Nb_6O_{19}]^{8-}$ increased by high loading of $[Nb_6O_{19}]^{8-}$ and efficiently promoted the hydrogenation of carbamate intermediates at the interface.

Applicability for the other secondary amines were confirmed using piperazine, methylpiperazine, 1,2,3,4-tetrahydroisoquinoline, and morpholine as substrates (**Scheme 2** and **Table 2**). *N*-formation proceeded when using other secondary amines. Note that hydrogenation of aromatic rings also proceeded when using 1,2,3,4-tetrahydroisoquinoline as a substrate, since the Pt atoms were exposed on the surface of $[Nb_6O_{19}]^{8-}$-modified Pt NPs. **Table S1** summarizes the catalytic activity for *N*-formylation reaction of secondary amines in the reported systems. The turnover frequency (TOF) of *N*-formylation of piperidine and morpholine over **4.0Nb6-Pt/Al$_2$O$_3$** based on the contained Pt atoms was 0.14 h^{-1} and 0.20 h^{-1}, respectively. K-salts of $[Pt(Nb_6O_{19})_2]^{12-}$ reported in our previous paper showed the higher TOF values.[7] In the paper, 2-3 nm of Pt NPs supported on NbO_x formed during the reaction and the surface decollated with Nb oxide clusters. On the other hand, since the Pt NPs of **4.0Nb6-Pt/Al$_2$O$_3$** were exposed to the surface after the $[Nb_6O_{19}]^{8-}$ modification, **4.0Nb6-Pt/Al$_2$O$_3$** resulted in lower TOF values. These also indicated the modification density of $[Nb_6O_{19}]^{8-}$ also important to promote the *N*-formylation reaction. As shown in **Tables S1**, almost all systems require the addition of external base to efficiently promote the reaction. However, **4.0Nb6-Pt/Al$_2$O$_3$** worked without addition of external base due to the basicity of modified $[Nb_6O_{19}]^{8-}$. Moreover, the dependence of modified $[Nb_6O_{19}]^{8-}$ amount on the catalytic activity (**Figure 4**) indicates that interface between basic $[Nb_6O_{19}]^{8-}$ and Pt NPs were essential for

the efficient reaction. One reason is the basic surface oxygen atoms stabilized carbamate ion intermediates. Other possibility is that the interface between basic $[Nb_6O_{19}]^{8-}$ and Pt NPs efficiently promotes the H_2 activation.

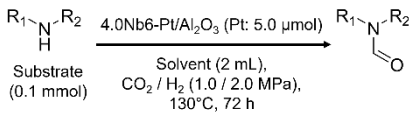

Scheme 2. *N*-Formylation of secondary amines using CO_2 as a carbon source.

Table 2. Substrate scope of *N*-formylation reaction of secondary amines using CO_2 over **4.0Nb6-Pt/Al_2O_3**.

Entry	Substrate	Yields of products (%)
1[a]	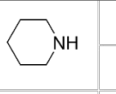	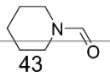 43
2[a]	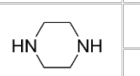	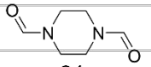 24
3[a]	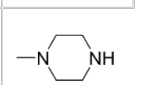	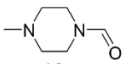 13
4[a]	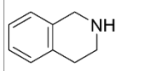	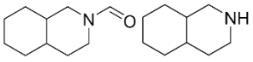 35 24
5[b]	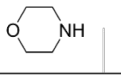	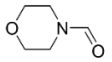 71

[a]Amines, 0.1 mmol; methanol, 2 mL; catalyst, 19.5 mg; internal standard, dodecane; CO_2, 1.0 MPa; H_2, 2.0 MPa; reaction temperature, 130°C; reaction time, 72 h.

[b]Dimethylamine was used as a solvent instead of MeOH.

Conclusions

In summary, we found that the *N*-formylation reaction using CO_2 as a carbon source proceeded efficiently via cooperation between the reducing ability of the supported Pt NPs and the basicity of the modified POM. The catalysts were prepared by a simple adsorption method in which Al_2O_3-supported Pt NPs were dispersed in $K_8Nb_6O_{19}$ aq. The modified $[Nb_6O_{19}]^{8-}$ was highly selectively adsorbed on Pt NPs rather than Al_2O_3 support while maintaining the basicity of $[Nb_6O_{19}]^{8-}$. Moreover, the IR-DRIFT using CO as a probe confirmed the electrodonation from $[Nb_6O_{19}]^{8-}$ to the Pt NP surface. $[Nb_6O_{19}]^{8-}$-modified Al_2O_3-supported Pt NPs afforded *N*-formylation products of various secondary types, even in the absence of an external base. The modified amounts of $[Nb_6O_{19}]^{8-}$ were saturated at ca.1.3wt_{Nb}%, even at a high concentration of $K_8Nb_6O_{19}$ aq., and the Pt NP surface remained exposed. The activity increased with increasing modified amounts of $[Nb_6O_{19}]^{8-}$, indicating that the interface of $[Nb_6O_{19}]^{8-}$ and Pt NPs was essential to the efficient reaction. From the dependence on the H_2 and CO_2 pressure, the hydrogenation of carbamate intermediates was the rate-determining step. The basic sites of surface oxygen atoms stabilize the carbamate intermediates near the Pt NP surface. This work that designed a Pt NP surface by a bottom-up modification with basic POMs facilitated the *N*-formylation reaction using CO_2 as a carbon source without the addition of any external base. Further developments in the POM adsorption method to increase the coverage should lead to the design of surfaces of metal NPs for efficient catalysis.

Author contributions

S.K. and S.Y. designed and supervised this study. Y.M. and S.F. contributed to all experimental work and data analysis. S. K. drafted the manuscript. All authors have given approval to the final version of the manuscript.

Conflicts of interest

The authors declare no conflicts of interest associated with this manuscript.

Data availability

The authors confirm that the data supporting the findings of this study are available within the article and its supplementary materials.

Acknowledgements

This research was financially supported by the New Energy and Industrial Technology Development Organization (NEDO, No. P14004), Japan Science and Technology Agency (JST) ACT-X (No. JPMJAX23D7), Japan Society for the Promotion of Science (JSPS) KAKENHI (Nos. 22K14543, 24K01259, 24K17562, and 24H02217 in Transformative Research Areas (A) JP24A202 Integrated Science of Synthesis by Chemical Structure Reprogramming), Joint Usage/Research Center for Catalysis (proposal 23DS0482 and 24DS0606), the Collaborative Research Program of Institute for Chemical Research, Kyoto University (grant #2023-127), Special Project by Institute for Molecular Science (IMS program 22IMS1262), Tokyo Human Resources Fund for City Diplomacy, Tokyo Metropolitan University Research Fund for Young Scientists, and Tokyo Metropolitan Government Advanced Research (R3-1). The XAFS experiments were performed with the approval of BL01B1 of SPring-8 (proposal nos. 2021A1406, 2021B1535, 2022A1627, 2022B1684, 2022B1911, 2022B0593, 2023A1554, 2023A1752, and 2023A1915).

Notes and references

1. Rogelj, J.; Den Elzen, M.; Höhne, N.; Fransen, T.; Fekete, H.; Winkler, H.; Schaeffer, R.; Sha, F.; Riahi, K.; Meinshausen, M. Paris Agreement Climate Proposals Need a Boost to Keep Warming Well Below 2C. *Nature* 2016, **534**, 631–639.

2. Honda, M.; Suzuki, A.; Noorjahan, B.; Fujimoto, K.-i.; Suzuki, K.; Tomishige, K. Low Pressure CO_2 to Dimethyl Carbonate by the Reaction with Methanol Promoted by Acetonitrile Hydration. *Chem. Commun.* 2009, 4596–4598.

3. Mikkelsen, M.; Jørgensen, M.; Krebs, F. C. The Teraton Challenge. A Review of Fixation and Transformation of Carbon Dioxide. *Energy Environ. Sci.* 2010, **3**, 43–81.
4. Appel, A. M.; Bercaw, J. E.; Bocarsly, A. B.; Dobbek, H.; DuBois, D. L.; Dupuis, M.; Ferry, J. G.; Fujita, E.; Hille, R.; Kenis, P. J. Frontiers, Opportunities, and Challenges in Biochemical and Chemical Catalysis of CO_2 Fixation. *Chem. Rev.* 2013, **113**, 6621–6658.
5. Li, Y.; Fang, X.; Junge, K.; Beller, M. A General Catalytic Methylation of Amines Using Carbon Dioxide. *Angew. Chem. Int. Ed.* 2013, **52**, 9568–9571.
6. Liu, Q.; Wu, L.; Jackstell, R.; Beller, M. Using Carbon Dioxide as a Building Block in Organic Synthesis. *Nat. Commun.* 2015, **6**, 5933.
7. Chudatemiya, V.; Kikkawa, S.; Hirayama, J.; Takahata, R.; Teranishi, T.; Tamura, M.; Yamazoe, S. Bifunctional Platinum‐Incorporated Polyoxoniobate Derived Catalyst for *N*-Formylation of Piperidine Using CO_2. *Asian J. Org. Chem.* 2022, **12**, e202200521.
8. Tamura, M.; Nakagawa, Y.; Tomishige, K. Direct CO_2 transformation to aliphatic polycarbonates. *Asian J. Org. Chem.* 2022, **11**, e202200445.
9. He, Z.; Liu, H.; Liu, H.; Qian, Q.; Meng, Q.; Mei, Q.; Han, B. Heterogeneous Cobalt-Catalyzed Direct *N*-Formylation of Isoquinolines with CO_2 and H_2. *ChemCatChem* 2017, **9**, 1947–1952.
10. Liu, H.; Mei, Q.; Xu, Q.; Song, J.; Liu, H.; Han, B. Synthesis of Formamides Containing Unsaturated Groups by *N*-Formylation of Amines Using CO_2 with H_2. *Green Chem.* 2017, **19**, 196–201.
11. Zhang, Y.; Wang, H.; Yuan, H.; Shi, F. Hydroxyl Group-Regulated Active Nano-Pd/C Catalyst Generation via in Situ Reduction of $Pd(NH_3)_xCl_y$/C for *N*-Formylation of Amines with CO_2/H_2. *ACS Sustain. Chem. Eng.* 2017, **5**, 5758–5765.
12. Li, J.; Li, C.; Feng, S.; Zhao, Z.; Zhu, H.; Ding, Y. Atomically Dispersed Zn-N_x Sites in N-Doped Carbon for Reductive *N*-Formylation of Nitroarenes with Formic Acid. *ChemCatChem* 2020, **12**, 1546–1550.
13. Cheng, D.; Wang, M.; Tang, L.; Gao, Z.; Qin, X.; Gao, Y.; Xiao, D.; Zhou, W.; Ma, D. Catalytic Synthesis of Formamides by Integrating CO_2 Capture and Morpholine Formylation on Supported Iridium Catalyst. *Angew. Chem. Int. Ed.* 2022, **134**, e202202654.
14. Ma, Y.; Chen, C.; Jiang, Y.; Wei, X.; Liu, Y.; Liao, H.; Wang, H.; Dai, S.; An, P.; Hou, Z. Ruthenium Single-Atom Anchored in Polyoxometalate-Ionic Liquids for *N*-Formylation of Amines with CO_2 and H_2. *ACS Catal.* 2023, **13**, 10295–10308.
15. Cheng, D.; Wang, M.; Yu, S.; Peng, M.; Zhou, W.; Yang, W.; Wang, M.; Ma, D. Reversible Hydrogenation of CO_2 to Formamides Using an Atomically Dispersed Ir/C_3N_4 Catalyst. *ACS Catal.* 2024, **14**, 5109–5115.
16. Dai, X.; Li, T.; Wang, B.; Kreyenschulte, C.; Bartling, S.; Liu, S.; He, D.; Yuan, H.; Bruckner, A.; Shi, F.; et al. Tailoring Active Cu_2O/Copper Interface Sites for *N*-Formylation of Aliphatic Primary Amines with CO_2/H_2. *Angew. Chem. Int. Ed.* 2023, **62**, e202217380.
17. Zou, Q.; Chen, J.; Wang, Y.; Gu, J.; Liu, F.; Zhao, T. Synthesis of Mesoporous Pd_xCu_{1-x}/Al_2O_{3-y} Bimetallic Catalysts via Mechanochemistry for Selective *N*-Formylation of Amines with CO_2 and H_2. *ACS Sustain. Chem. Eng.* 2021, **9**, 16153–16162.
18. Mitsudome, T.; Urayama, T.; Fujita, S.; Maeno, Z.; Mizugaki, T.; Jitsukawa, K.; Kaneda, K. A Titanium Dioxide Supported Gold Nanoparticle Catalyst for the Selective *N*-Formylation of Functionalized Amines with Carbon Dioxide and Hydrogen. *ChemCatChem* 2017, **9**, 3632–3636.
19. Hidaka, M.; Lin, M.; Yamakawa, H.; Nakayama, A.; Murayama, T.; Shimada, T.; Takagi, S.; Ishida, T. Au/Nb_2O_5-Catalyzed *N*-Formylation of Amines Utilizing High Selectivity to Formate Intermediate in CO_2 Hydrogenation. *Chem. Lett.* 2023, **52**, 874–877.
20. Zhang, M.; Hao, J.; Neyman, A.; Wang, Y.; Weinstock, I. A. Influence of Polyoxometalate Protecting Ligands on Catalytic Aerobic Oxidation at the Surfaces of Gold Nanoparticles in Water. *Inorg. Chem.* 2017, **56**, 2400–2408.
21. Leiser, S. S.; Polin, L.; Gan-Or, G.; Raula, M.; Weinstock, I. A. Hexaniobate Cluster Anion Monolayers on Gold Nanoparticles: A New Structural Role for Alkali Metal Countercations. *Inorg. Chem.* 2019, **58**, 1012–1015.
22. Neyman, A.; Meshi, L.; Zeiri, L.; Weinstock, I. A. Direct Imaging of the Ligand Monolayer on an Anion-Protected Metal Nanoparticle Through Cryogenic Trapping of its Solution-State Structure. *Journal of the American Chemical Society* 2008, **130**, 16480-16481.
23. Kikkawa, S.; Fukuda, S.; Hirayama, J.; Shirai, N.; Takahata, R.; Suzuki, K.; Yamaguchi, K.; Teranishi, T.; Yamazoe, S. Dual Functional Catalysis of $[Nb_6O_{19}]^{8-}$-Modified Au/Al_2O_3. *Chem. Commun.* 2022, **58**, 9018–9021.
24. Xia, K.; Yatabe, T.; Yonesato, K.; Yabe, T.; Kikkawa, S.; Yamazoe, S.; Nakata, A.; Yamaguchi, K.; Suzuki, K. Supported Anionic Gold Nanoparticle Catalysts Modified Using Highly Negatively Charged Multivacant Polyoxometalates. *Angew. Chem. Int. Ed.* 2022, **61**, e202205873.
25. Xia, K.; Yatabe, T.; Yonesato, K.; Kikkawa, S.; Yamazoe, S.; Nakata, A.; Ishikawa, R.; Shibata, N.; Ikuhara, Y.; Yamaguchi, K.; et al. Ultra-Stable and Highly Reactive Colloidal Gold Nanoparticle Catalysts Protected Using Multi-Dentate Metal Oxide Nanoclusters. *Nat. Commun.* 2024, **15**, 851.
26. Martin, C.; Kastner, K.; Cameron, J. M.; Hampson, E.; Alves Fernandes, J.; Gibson, E. K.; Walsh, D. A.; Sans, V.; Newton, G. N. Redox-Active Hybrid Polyoxometalate-Stabilised Gold Nanoparticles. *Angew. Chem. Int. Ed.* 2020, **59**, 14331–14335.
27. Hayashi, S.; Sasaki, N.; Yamazoe, S.; Tsukuda, T. Superior Base Catalysis of Group 5 Hexametalates $[M_6O_{19}]^{8-}$ (M= Ta, Nb) over Group 6 Hexametalates $[M_6O_{19}]^{2-}$ (M= Mo, W). *J. Phys. Chem. C* 2018, **122**, 29398–29404.
28. Kikkawa, S.; Fujiki, Y.; Chudatemiya, V.; Nagakari, H.; Shibusawa, K.; Hirayama, J.; Nakatani, N.; Yamazoe, S. Water-Tolerant Superbase Polyoxometalate $[H_2(Nb_6O_{19})]^{6-}$ for Homogeneous Catalysis. *Angew. Chem. Int. Ed.* 2024, **63**, e202401526.
29. Hayashi, S.; Yamazoe, S.; Koyasu, K.; Tsukuda, T. Application of Group V Polyoxometalate as an Efficient Base Catalyst: a Case Study of Decaniobate Clusters. *RSC Adv.* 2016, **6**, 16239–16242.
30. Hayashi, S.; Yamazoe, S.; Koyasu, K.; Tsukuda, T. Lewis Base Catalytic Properties of $[Nb_{10}O_{28}]^{6-}$ for CO_2 Fixation to Epoxide: Kinetic and Theoretical Studies. *Chem. Asian. J.* 2017, **12**, 1635–1640.
31. Blyholder, G. Molecular Orbital View of Chemisorbed Carbon Monoxide. *J. Phys. Chem.* 1964, **68**, 2772–2777.
32. Kikkawa, S.; Teramura, K.; Asakura, H.; Hosokawa, S.; Tanaka, T. Isolated Platinum Atoms in Ni/γ-Al_2O_3 for Selective Hydrogenation of CO_2 toward CH_4. *J. Phys. Chem. C* 2019, **123**, 23446-23454.

Data availability statements

The data supporting this article have been included as part of the Supplementary Information.